

Evaluation of intervertebral disc cartilaginous endplate structure using magnetic resonance imaging

Sung M. Moon · Jonathon H. Yoder ·
Alexander C. Wright · Lachlan J. Smith ·
Edward J. Vresilovic · Dawn M. Elliott

Received: 13 December 2011 / Revised: 1 March 2013 / Accepted: 25 April 2013 / Published online: 15 May 2013
© Springer-Verlag Berlin Heidelberg 2013

Abstract

Purpose The cartilaginous endplate (CEP) is a thin layer of hyaline cartilage positioned between the vertebral endplate and nucleus pulposus (NP) that functions both as a mechanical barrier and as a gateway for nutrient transport into the disc. Despite its critical role in disc nutrition and degeneration, the morphology of the CEP has not been well characterized. The objective of this study was to visualize and report observations of the CEP three-dimensional morphology, and quantify CEP thickness using an MRI FLASH (fast low-angle shot) pulse sequence.

Methods MR imaging of ex vivo human cadaveric lumbar spine segments ($N = 17$) was performed in a 7T MRI scanner with sequence parameters that were selected by utilizing high-resolution T1 mapping, and an analytical MRI signal model to optimize image contrast between CEP and NP. The CEP thickness at five locations along the mid-sagittal AP direction (center, 5 mm, 10 mm off-center towards anterior and

posterior) was measured, and analyzed using two-way ANOVA and a post hoc Bonferonni test. For further investigation, six in vivo volunteers were imaged with a similar sequence in a 3T MRI scanner. In addition, decalcified and undecalcified histology was performed, which confirmed that the FLASH sequence successfully detected the CEP.

Results CEP thickness determined by MRI in the mid-sagittal plane across all lumbar disc levels and locations was 0.77 ± 0.24 mm ex vivo. The CEP thickness was not different across disc levels, but was thinner toward the center of the disc.

Conclusions This study demonstrates the potential of MRI FLASH imaging for structural quantification of the CEP geometry, which may be developed as a technique to evaluate changes in the CEP with disc degeneration in future applications.

Keywords Cartilaginous endplate · Endplate morphology · Intervertebral disc · Magnetic resonance imaging (MRI)

S. M. Moon · J. H. Yoder · L. J. Smith
Department of Orthopaedic Surgery, University
of Pennsylvania, Philadelphia, PA, USA

S. M. Moon
MR Systems, GE Healthcare, Florence, SC, USA

A. C. Wright
Department of Radiology, University of Pennsylvania,
Philadelphia, PA, USA

E. J. Vresilovic
Department of Orthopaedics and Rehabilitation,
Penn State University, Hershey, PA, USA

D. M. Elliott (✉)
Department of Biomedical Engineering, University of Delaware,
125 E. Delaware Ave., Newark, DE 19716, USA
e-mail: delliottd@udel.edu

Introduction

The intervertebral disc is the largest avascular tissue in the body, undergoes more extensive changes with age and degeneration than any other tissue [1, 2], and is associated with low back pain [3–5]. The intervertebral disc has three distinct anatomical regions: the central nucleus pulposus (NP), the fibrocartilaginous annulus fibrosus, and, superiorly and inferiorly, two cartilaginous endplates (CEP). These CEPs are distinct from the adjacent vertebral endplates, which are composed of cortical bone [6–8]. The CEP is an approximately 600- μ m thick layer of hyaline cartilage positioned between the vertebral endplate and NP [7]. It functions both as a mechanical barrier between the

pressurized NP and the vertebral bone, as well as a gateway for nutrient transport into the disc from adjacent blood vessels [9–12]. With intervertebral disc degeneration, the CEP becomes sclerotic, loses vascular contact, and exhibits decreased permeability [13–19]. This process is considered to contribute to disc degeneration by reducing the diffusion of nutrients to the cells of the NP [6, 20–22]. Identifying changes in CEP morphology may, therefore, be important for the diagnosis and prognosis of intervertebral disc health. Despite this, the morphology of the CEP and how it changes with disc aging and degeneration have not been well characterized.

Magnetic resonance imaging (MRI) is a non-invasive, non-ionizing imaging modality well known for its superior soft tissue contrast, making it ideal for disc applications including anatomy, composition, and stage of degeneration through a number techniques (e.g., T1 ρ - and T2-weighted images) [23–27]. Application of MRI to the study of disc degeneration has to date focused predominantly on the NP and annulus fibrosus, with few studies examining the CEP. Moreover, current clinical routine diagnosis of disc health using MRI does not address the CEP due to limitations in spatial resolution as constrained by scan time, combined with the inability to distinguish between the thin CEP and adjacent NP and annulus fibrosus tissues.

Visualization of the thin cartilaginous endplates requires not only sufficiently high resolution (small voxels), but also short echo time (due to short T2 of the tissue), optimized sequence parameters that yield sufficient image contrast to distinguish each disc substructure, and fast scan time, especially for in vivo application. In this study, a T1-weighted 3D FLASH (fast low-angle shot) sequence was chosen due to its fast imaging time and suitability for in vivo application [28]. In the FLASH sequence, transverse magnetization is spoiled and the steady-state longitudinal magnetization depends on T1 and the flip angle. The sequence parameters repetition time (TR) and flip angle thus determine the T1 contrast in the FLASH sequence and were optimized in this study using an analytical model. Even with a very short TR , the FLASH sequence can provide high T1 contrast while preserving reasonable signal intensity in tissues with T2 equal to or longer than TR (e.g., CEP). UTE (ultra-short echo time) imaging also is able to visualize the CEP [29]. However, the UTE technique was not selected for this study because it is not readily available on clinical scanners and UTE generally requires a longer scan time than FLASH with short echo time for the same field of view and resolution, assuming the Nyquist sampling criterion is met.

The overall objective of this study was to evaluate the cartilaginous endplate structure by MRI using an optimized T1-weighted 3D FLASH sequence. Specifically, the first

aim was to visualize the three-dimensional morphology of the CEP in cadaveric human spine segments and to quantify its thickness using high-resolution 7T MRI. The second aim was to apply the technique in vivo using 3T MRI to assess the feasibility of future translation to the clinical setting.

Methods

Optimization of CEP image contrast

In order to attain pulse sequence parameters with optimized contrast in the CEP, MRI signal intensity and image contrast were simulated using an analytical MRI pulse sequence equation prior to imaging. The T1 contrast of the FLASH sequence is a function only of TR and flip angle in the limit of short echo time (TE), and the dependence of MRI signal intensity upon flip angle, TR , and T1 is given by

$$\text{MRI signal} = A \sin \alpha \frac{1 - \exp(-TR/T1)}{1 - \cos \alpha \exp(-TR/T1)}, \quad (1)$$

where A is the equilibrium magnetization reduced by T2 relaxation and α is the flip angle [30, 31]. This equation was used to analyze the signal dependence on flip angle and TR , which are the primary adjustable imaging parameters in this application.

The T1 values of NP and CEP for use in Eq. 1 were measured in a healthy cadaveric lumbar disc (Grade = 2.3) [25]. T1 was measured at both 7T and 3T magnetic field strength using a fully relaxed ($TR = 5,100$ ms) 2D spin echo inversion recovery pulse sequence with ten different inversion times ($TI = 33\text{--}5,000$ ms, $TE = 11/13$ ms (7T and 3T, respectively), in-plane resolution = $200 \times 200 \mu\text{m}^2$, slice thickness = 5 mm, matrix = 256×256 , and field of view = $5.1 \times 5.1 \text{ cm}^2$, Receiver Bandwidth (RBW) = 200 Hz/Px). Each pixel in these ten images with different inversion times was fitted with the exponential curve $I = I_0(1 - 2 \exp(-TI/T1))$ to yield a T1 map. Representative T1 values of NP and CEP were determined by averaging 900 or more pixels within each disc substructure (i.e., NP, annulus fibrosus, CEP).

Using the experimentally determined mean T1 and I_0 values for NP and CEP, normalized MRI signals (Eq. 1) for each substructure were plotted versus flip angle and TR . Also, the image contrast (signal difference) between NP and CEP (Δ_{CEP}), normalized to maximize the signal intensity of CEP, was plotted versus flip angle and TR for the full range of possible parameter values according to

$$\Delta_{\text{CEP}} = \left| \frac{\text{Signal}_{\text{NP}} - \text{Signal}_{\text{CEP}}}{1 - \text{Signal}_{\text{CEP}}} \right| \quad (2)$$

Ex vivo MRI imaging

Specimens were prepared from 11 cadaveric human lumbar spines ($n = 17$, age: 57.7 ± 13.3). While for some subjects 2–3 levels were used from a single spine, consistent with common practice in the literature [32–34], these discs were assumed to be independent samples and post hoc statistical analysis confirmed no subject dependence on CEP height. Each whole spine was first scanned with a mid-sagittal T2-weighted turbo spin echo imaging sequence for routine grading of degenerative state [25, 26]. The integer grade from five individual examiners was averaged (Grade: 2.8 ± 0.7). Lumbar spines were then dissected into bone-disc-bone segments with posterior elements removed and sealed in airtight freezer bags to avoid dehydration during imaging. The sealed segments were then embedded in 2 % agarose gel for immobilization and to reduce image distortion at tissue edges due to the tissue/air mismatch in magnetic susceptibility.

For protocol optimization, the flip angle and TR that providing the best optimal NP-CEP contrast were selected using the analytical model simulation. All ex vivo imaging with specimens was done in a Siemens Magnetom 7T scanner (Siemens Medical Solutions, Erlangen, Germany) using a 4-channel ankle coil (Insight MRI) [35]. Due to the thinness of the endplate, a voxel size of $200 \mu\text{m}^3$ was chosen. Imaging parameters for ex vivo scans were $TR = 9$ ms, $TE = 3.7$ ms, flip angle = 20° , $0.2 \times 0.2 \times 0.2 \text{ mm}^3$ isotropic resolution, matrix = 320×320 , field of view = $6.8 \times 6.8 \text{ cm}^2$, RBW = 200 Hz/Px, and 1 average with fat suppression. Scan time was 3 min per disc.

Histology

Histological analysis was performed to confirm that the structure visualized using MRI was indeed the CEP and to compare CEP measurements with measurements from site-matched MR images. Two adjacent 8 mm biopsy punches, comprising vertebral bone, the CEP and the NP, were taken from a disc (63 years, male, L2L3, Grade: 2.6), which had previously been imaged as described above, and a photograph of the specimen was taken. These $200 \mu\text{m}^3$ isotropic MRI data and the photograph later were co-registered to confirm the location of the punches. Both punches were fixed in buffered 10 % formalin overnight. One punch was then decalcified overnight in formic acid/EDTA. Twenty-micron sections were cut on a cryostat, and double stained with Alcian blue and picosirius red to demonstrate glycosaminoglycans and collagen, respectively, and imaged using bright field microscopy. The other punch was sectioned in a similar way, but without prior decalcification. These sections were then stained using the von Kossa method to demonstrate calcium deposits and imaged using

differential interference contrast microscopy (Eclipse 90i; Nikon; Tokyo, Japan). To compare MRI-based CEP measurements with a histological standard, three 4-mm diameter CEP samples were punched within the inferior endplate for a single disc (75 years, male, L2L3, Grade: 2.0), sectioned on a cryostat, and the CEP thickness measured at three evenly spaced intervals across the plug. Virtual plugs were generated from the MR data by co-registering with a photograph of the vertebral surface and site-matched CEP thickness measurements were made.

In vivo MRI study

An in vivo volunteer study ($N = 6$, age: 32.0 ± 4.2 , Grade: 2.2 ± 0.4) was performed to assess feasibility of clinical application. All in vivo scans were done in a 3T Siemens Tim Trio (Siemens Medical Solutions, Erlangen, Germany) with Siemens spine array and body matrix RF coils. Similar to the ex vivo study, a routine T2-weighted mid-sagittal turbo spin echo image was acquired first to determine the degenerative grade of each lumbar disc (slice thickness = 5.0 mm, $TR = 4,540$ ms, $TE = 123$ ms, flip angle = 160° , matrix = 251×256 , field of view = $25 \times 25 \text{ cm}^2$, in-plane resolution $\approx 1 \times 1 \text{ mm}^2$, RBW = 130 Hz/Px, 2 averages). The 3D FLASH image was then acquired with imaging parameters as follows: slice thickness = 5.0 mm, $TR = 9.0$ ms, $TE = 3.7$ ms, flip angle = 20° , matrix = 504×576 , field of view = $20 \times 23 \text{ cm}^2$, in-plane resolution $\approx 0.4 \times 0.4 \text{ mm}^2$, RBW = 202 Hz/Px, and 1 average. Total imaging time for both T2 and FLASH scans was 13 min, covering the entire lumbar spine. After scanning, the T2-weighted mid-sagittal image was registered to the FLASH image and displayed as color overlay (a fusion image) using OsiriX software [36] to identify the relative locations of the CEP and the NP.

Quantification of endplate height

Images from both ex vivo and in vivo datasets were imported into OsiriX software and evaluated for CEP contrast in comparison to the surrounding structures, for morphology in two-dimensions (in vivo) and three-dimensions (ex vivo), and for CEP thickness ex vivo. Ex vivo MRI data had isotropic resolution and, therefore, could be viewed in arbitrary image planes using multi-planar reformatting. The CEP thickness was measured for the superior and inferior CEP along the mid-sagittal plane at five locations (center, 5 and 10 mm off the center towards anterior and 5 and 10 mm off the center towards posterior). Average thicknesses across specimens were calculated for each location and each disc level.

The CEP thickness measurements from ex vivo scans were evaluated using a two-way ANOVA with repeated

measures, where the factors were disc level (L1L2, L2L3, L3L4, L4L5, L5S1) and anterior-posterior disc location (center, 5 and 10 mm off the center towards anterior, and 5 and 10 mm off the center towards posterior). Significance was set at $p < 0.05$. A post hoc Bonferonni test was performed when significance was detected resulting in significance at $p < 0.005$.

Results

A T1 map obtained at 7T and the average T1 values (\pm standard deviation) of each disc substructure obtained at 7T and 3T are presented for a healthy disc (Fig. 1). These T1 values were used in Eqs. 1 and 2 to calculate signal intensity and determine optimal pulse sequence parameters for NP-CEP image contrast (Δ_{CEP}) (Fig. 2). Figure 2a shows a contour plot of Δ_{CEP} covering the exhaustive range of flip angles (0–180°) and TR values (0–6,000 ms). However, only a small region corresponding to short TR (dotted box in Fig. 2a), where scan time is reasonable for in vivo applications, was considered for selecting the optimal sequence parameters (Fig. 2b), and the optimal flip angle and TR were identified (asterisk in Fig. 2b). A flip angle of 20° with a TR of 9 ms yielded the highest contrast between the CEP and NP (Fig. 2c, d). Note that even though a flip angle of 3° yields higher signal difference between the NP and CEP; this was not chosen because for angles less than 5° the MR signal changes rapidly, resulting in a smaller range of optimal image contrast. Furthermore, at 5° or less the absolute signal intensity of the CEP is lower than it is at 20°.

The optimized T1-weighted 3D FLASH sequence yielded good contrast between the NP and CEP (Fig. 3). The images showed clear distinction of the CEP (arrows). Multi-planar reformatting was done to elucidate the three-dimensional extent and overall shape of the CEP, making use of the high-resolution and isotropic nature of all the ex vivo datasets. Mean projections of an axial slab (1.3 mm) of the CEP showed that the shape and size of the CEP can vary considerably between specimens (Fig. 3).

Histology confirmed that the structures observed in MR images were indeed CEP (locations of histological samples are shown in Fig. 4a, b). Alcian blue and picrosirius red histology successfully illustrated different anatomic regions (i.e., trabecular bone, bony endplate, CEP, and NP) (Fig. 4c). Von Kossa staining showed calcification of the adjacent vertebral trabecular bone and a very thin layer of cortical bone; however, with the exception of a very small number of cell lacunae at the bony interface, there was no calcification within the CEP itself (Fig. 4d). To address accuracy of our MRI-based CEP thickness quantitative measurements of CEP thickness made from histological sections were 0.42 ± 0.69 mm. These CEP dimensions were of the same magnitude to those measured using MRI on site-matched virtual plugs, which were 0.45 ± 0.12 mm.

In an effort to translate this new technique into in vivo applications, a healthy volunteer study was performed. A representative image from a 38-year-old male volunteer is presented (Fig. 5). The CEP is not visible in the conventional T2-weighted mid-sagittal image, typically used clinically to evaluate the disc (Fig. 5a). The FLASH image with optimized parameters, however, highlights the CEP well (Fig. 5b). The fusion image shows that the high-intensity regions (arrowheads) in Fig. 5a are not co-localized with the cartilaginous endplates (Fig. 5c).

The thickness of the CEP at the mid-sagittal plane and its correlation with disc level and anterior-posterior location were evaluated in the specimen MRI data. Across all disc levels and locations, the mean CEP thickness was 0.77 ± 0.24 mm similar to that of [7] 0.62 ± 0.29 mm. No significant difference in CEP thickness was observed across disc levels (Fig. 6a). There were significant effects of anterior–posterior location on CEP thickness (Fig. 6b), where the minimum thickness was at the center of the disc (0.54 ± 0.12 mm, averaged across all lumbar levels). The thickness at the center was 23 % less than the 0.5 cm anterior–posterior location and 44 % less than the 1.0 cm anterior–posterior location ($p < 0.005$), resulting in a “V” shaped pattern across the disc (Fig. 6b). There was no statistical interaction between level and anterior-posterior location for the CEP thickness measurements.

Fig. 1 T1 map of a healthy disc, obtained at 7T (scale bar in ms). The table shows mean T1 values within each disc substructure, obtained at both 7T and 3T. AF annulus fibrosus

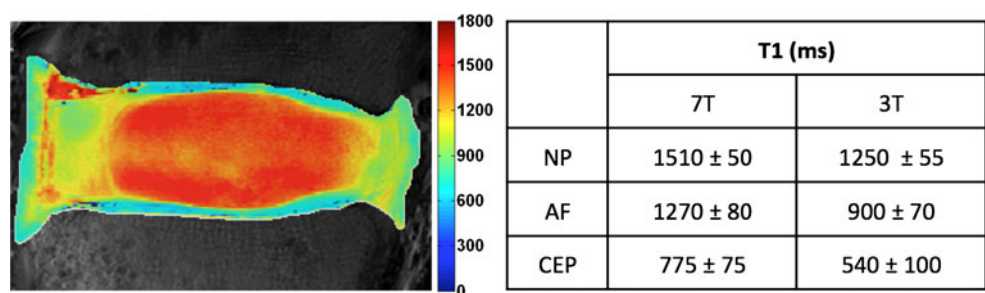
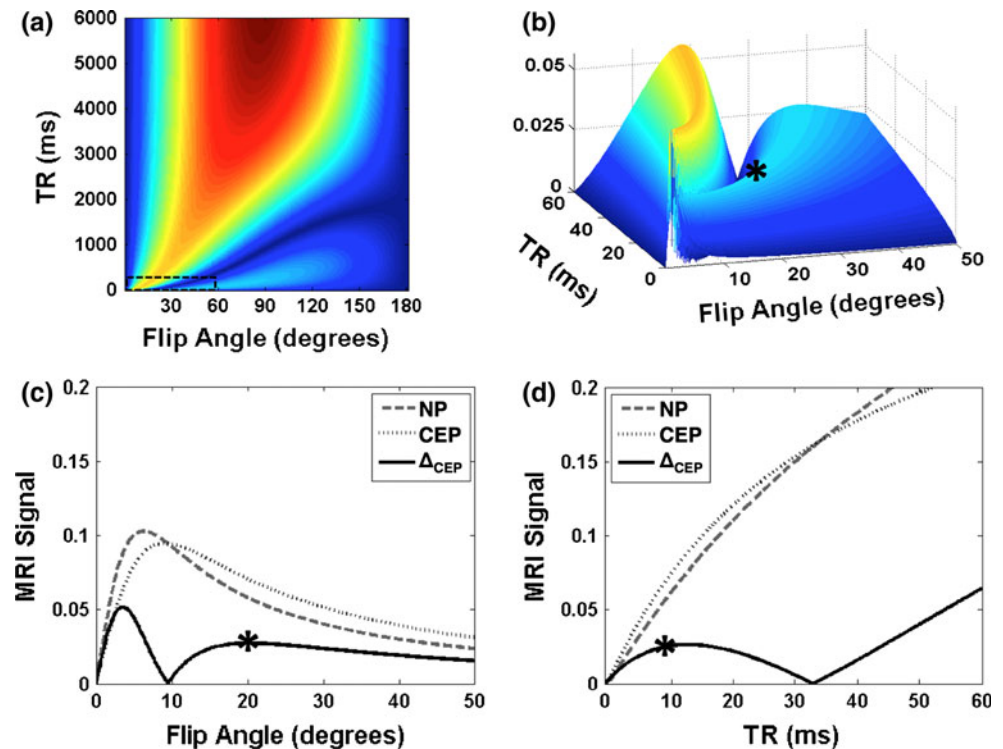


Fig. 2 Computed MRI signals and image contrast at 7T. **a** NP-CEP image contrast (Δ_{CEP}), according to Eq. 2, over the full range of the parameters flip angle and TR. **b** Close-up 3D view within the *small dashed box* in (a). Asterisk (*) indicates the point chosen as optimal. **c, d** Computed NP (*dashed*) and CEP (*dotted*) MRI signals, and image contrast (Δ_{CEP} , *solid*) versus flip angle at optimal TR (9 ms) (c) and versus TR at optimal flip angle (20°) (d)



Discussion

This study visualized the CEP morphology in three dimensions and quantified CEP thickness using an MRI 3D FLASH sequence. Optimal sequence parameters were selected by utilizing high-resolution T1 mapping and an analytical MRI signal model to maximize the signal contrast between the CEP and NP. In addition, histology was performed which confirmed that the MRI FLASH sequence successfully detected the CEP and provided an accurate measurement of CEP thickness. Our MRI FLASH microstructural observations are consistent with recent ultrashort echo time MR imaging of uncalcified and calcified CEP [37] although that study did not measure CEP thickness. The CEP thickness measured in the mid-sagittal plane both *ex vivo* and *in vivo* gave similar results, showing no effect of level, but the CEP becomes thinner toward the center of the disc. This study demonstrates the potential of MRI FLASH imaging for structural quantification of the CEP geometry, which may be developed as a technique to evaluate changes in CEP with disc degeneration in future applications.

T1 mapping and an analytical model of image contrast proved valuable in selecting parameters for FLASH imaging to emphasize the CEP. The high-resolution T1 map showed significant differences in T1 values between the NP and CEP, allowing these structures to be distinguished using appropriate sequence parameters. However, the T1 of the annulus fibrosus was closer to that of the CEP

than to that of the NP; thus, careful choice of scan parameters would be needed to distinguish the CEP from the annulus fibrosus. Although only one representative disc was used to obtain the T1 map for the simulations to select the flip angle and TR, the selected optimal parameters resulted in excellent contrast for most of the specimens and volunteers. The NP-CEP contrast using optimized parameters from the analytical model would vary as T1 and T2 are expected to vary depending upon the subject's disc health.

The MRI FLASH images using optimized parameters yielded complete and detailed 3D morphology of the CEP, and its axial, sagittal, and coronal views were shown for the first time. The size and shape of the CEP varied considerably among subjects and disc levels. In particular, the circumference of the CEP as seen in the axial sections often had an irregular edge, and this may be an indication of CEP calcification associated with disc degeneration. Additional work is needed to evaluate this, however, as the histological samples prepared in this study did not contain calcification within the CEP. While preliminary, and of small sample size, the results suggest CEP morphology may be related to disc level and disc health. However, more samples across a large range of degeneration will be required before such correlations can be tested.

In order to assess clinical feasibility, the FLASH technique was applied *in vivo* at 3T, demonstrating that the CEP was clearly visible (Fig. 5). The results were encouraging, considering the fact that SNR in the nucleus

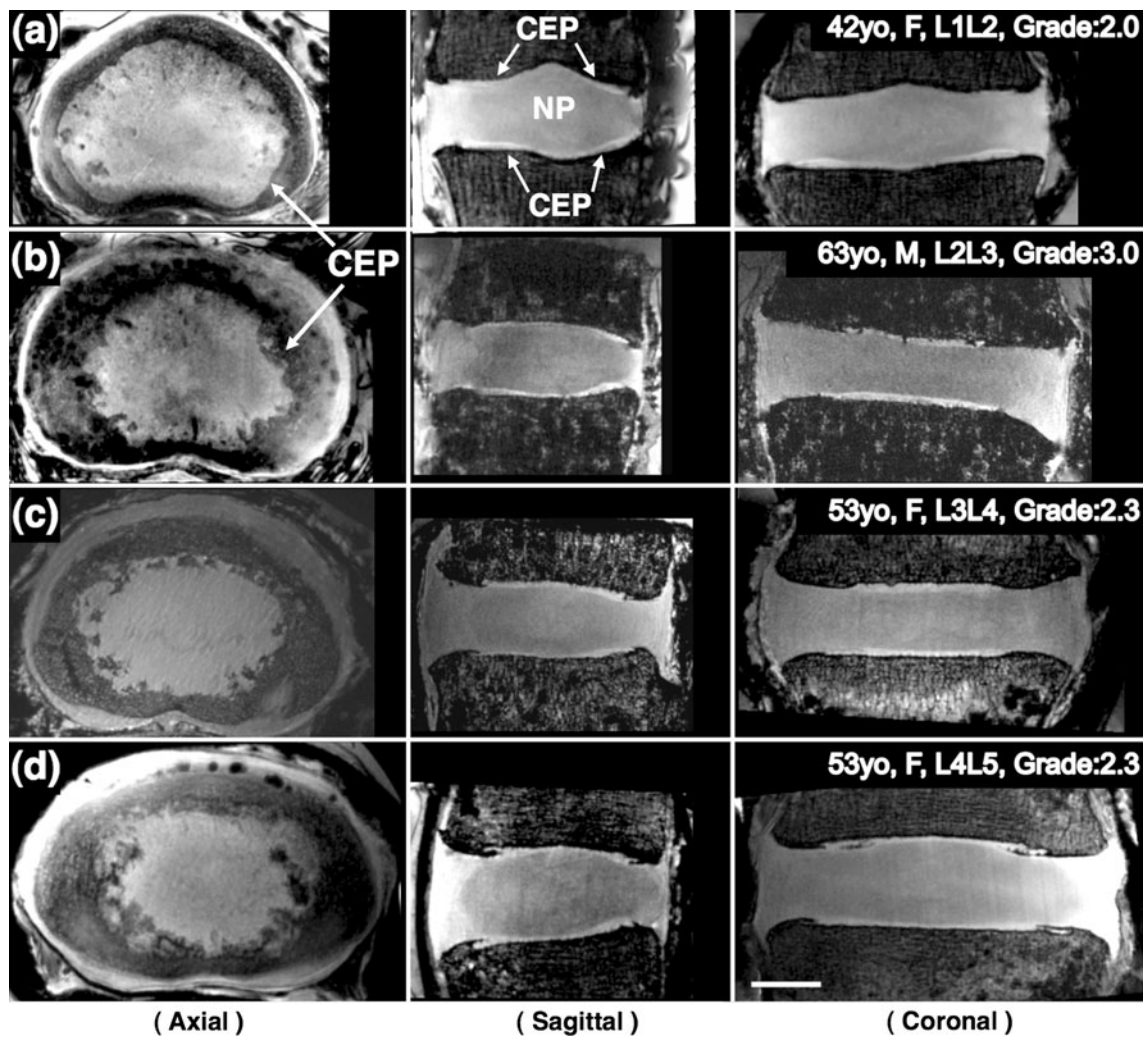


Fig. 3 MRI images of four different specimens with 200 μm isotropic resolution acquired at 7T. Three-plane views reformatted from the same isotropic dataset of each specimen clearly demonstrate the CEPs (arrows) clearly, which are located between the vertebral

body and the NP. Axial views show that the shape and size of the CEP can vary considerably for different subjects and levels: **a** 47 years, female, L1L2; **b** 63 years, male, L2L3; **c** 53 years, female, L3L4; **d** 53 years, female, L4L5. Scale bar = 1 cm

in vivo at 3T (≈ 16) was more than two times less than ex vivo at 7T (≈ 45). While SNR is proportional to field strength, for the case where the image noise is dominated by the sample, it is also proportional to voxel size and depends on factors such as T1, T2, pulse sequence parameters, and the type of RF coil used. In Fig. 5, lack of CEP visibility in the conventional T2-weighted image, particularly in comparison to the FLASH image, can be explained in part by the different echo times between the two sequences. We confirmed this using a standard method for T2 measurement, i.e., 2D spin echo images acquired with a range of echo times to generate T2 maps of a disc, from which we found T2 of the CEP to be 19 ms at 3T and 14 ms at 7T, respectively. Therefore, most of the CEP signal had been lost by the time the echo was measured in the T2-weighted sequence (123 ms). However, in the FLASH sequence the echo time could be made sufficiently

fast (3.7 ms) to capture the short-T2 signal of the CEP. Moreover, ultra-short echo times were not necessary to achieve excellent CEP contrast. The use of a custom-made RF coil specifically designed for lumbar spines could help mitigate the SNR difference between 3T and 7T systems. Additionally, further optimization of the sequence may be required for future in vivo studies.

The measured CEP thicknesses agree well with previous literature, as does the V-shaped pattern along the anterior-posterior axis of the disc (Fig. 6b) [7]. Furthermore, there was no effect of disc level on CEP thickness. Future studies will develop a semi-automated analysis programs that will give measurements with less user input. We found similar trends in the in vivo images, although these were not reported here due to the limited number of samples. The voxel size in vivo was larger, which could lead to an overestimate of thickness due to partial volume averaging.

Fig. 4 MRI and histology images of the same specimen (63 years male, L2L3, Grade 2.6). Axial (a) and coronal (b) FLASH MRI of the whole disc, showing approximate locations of biopsy punches used for histological analysis. c Representative histology section of the CEP stained with Alcian blue (glycosaminoglycans) and picrosirius red (collagen), showing adjacent NP and vertebral bone. d Von Kossa staining of an undecalcified section, showing regions of bone distinct from CEP and minimal CEP calcification. (Scale bars in a and b = 1 cm and in c and d = 0.5 mm; VB vertebral bone)

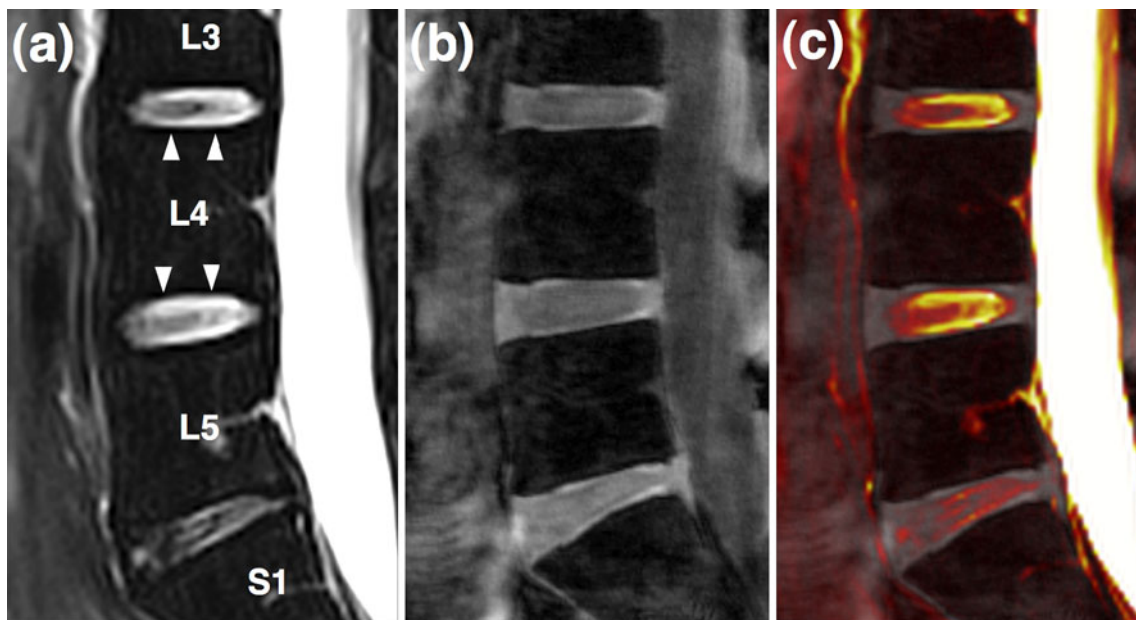
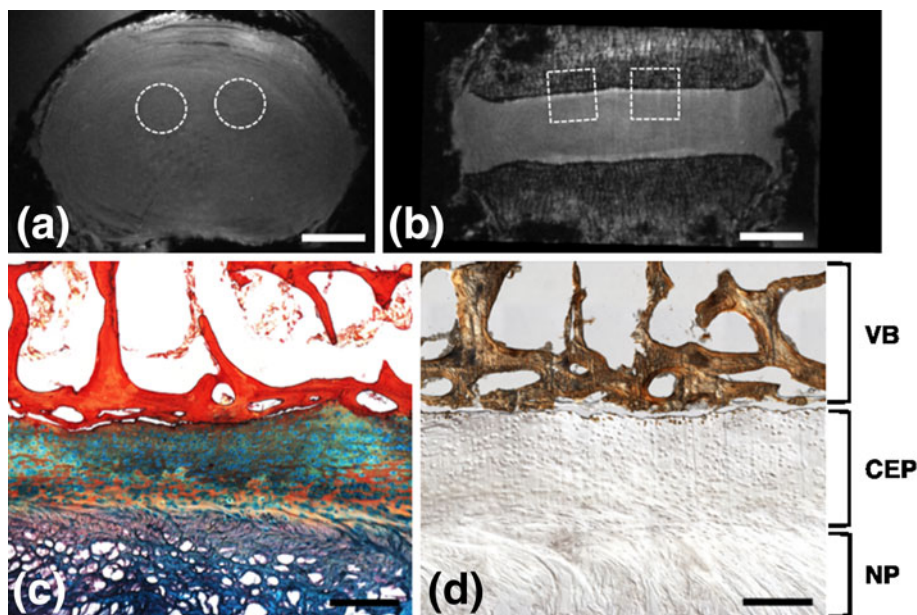
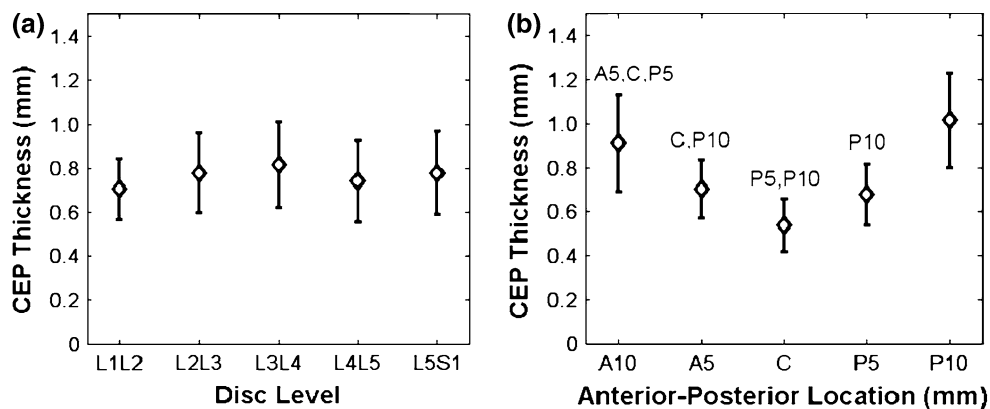


Fig. 5 In vivo data from a healthy volunteer obtained at 3T. a Routine T2-weighted mid-sagittal image b 3D FLASH image c fusion image of (a) and (b) showing that high-intensity regions (arrowheads) in image (a) are not co-localized with cartilaginous endplates

Fig. 6 CEP thicknesses in specimens, as measured on mid-sagittal MRI slices: a at different disc levels b at different anterior-posterior locations (C center, A5, A10 = 5 and 10 mm off the center towards anterior, P5, P10 = 5 and 10 mm off the center towards posterior). Letters on top of error bars indicate significance ($p < 0.005$) between measured locations



In any case, it is clear that due to both the thinness and curvature of the CEP voxel size should be minimized to avoid artifacts such as Gibbs ringing and partial volume averaging.

In conclusion, this study demonstrated CEP three-dimensional visualization using MRI, showing the three-dimensional CEP morphology and quantifying the CEP thickness in specimens. The CEP thickness was not related to disc level, but the CEP was significantly thicker in the periphery compared with the central location of the disc. The optimized MRI pulse sequence also was applied to human imaging in vivo, and the CEP exhibited similar trends to the ex vivo data. This work thus establishes a methodology for CEP MR imaging. With the relatively short in vivo scan time, the technique will provide a new tool for non-invasive assessment and quantification of disc health.

Acknowledgments This work is supported by NIH grants R01 AR058450 and R01 AR050052.

Conflict of interest None.

References

- Ferguson SJ, Steffen T (2003) Biomechanics of the aging spine. *Eur Spine J* 12:S97–103
- Adams MA, Dolan P (2005) Spine biomechanics. *J Biomech* 38:1972–1983
- Louma K, Riihimaki H, Luukkonen R et al (2000) Low back pain in relation to lumbar disc degeneration. *Spine* 24:487–492
- Peng B, Hou S, Wu W et al (2006) The pathogenesis and clinical significance of a high-intensity zone (HIZ) of lumbar intervertebral disc on MR imaging in the patient with discogenic low back pain. *Eur Spine J* 15:583–587
- Videman T, Nurminen M (2004) The occurrence of annular tears and their relation to lifetime back pain history: a cadaveric study using barium sulfate discography. *Spine* 29:2668–2676
- Raj PP (2008) Intervertebral disc: anatomy-physiology-pathophysiology-treatment. *Pain Practice* 8:18–44
- Roberts S, Menage J, Urban JPG (1989) Biomechanical and structural properties of the cartilage end-plate and its relation to the intervertebral disc. *Spine* 14:166–174
- Francois RJ, Bywaters EGL, Aufdermaur M (1985) Illustrated glossary for spinal anatomy. *Rheumatol Int* 5:241–245
- Crock HV, Goldwasser M (1984) Anatomic studies of the circulation in the region of the vertebral end-plate in adult greyhound dogs. *Spine* 9:702–706
- Roberts S, Menage J, Einstein SM (1993) The cartilage end-plate and intervertebral disc in scoliosis: calcification and other sequelae. *J Ortho Res* 11:747–757
- Moore RJ (2000) The vertebral end-plate: what do we know? *Eur Spine J* 9:92–96
- Urban JPG, Roberts S (2003) Degeneration of the intervertebral disc. *Arthr Res Therapy* 5:120–130
- Grignon B, Grignon Y, Mainard D et al (2000) The structure of the cartilaginous end-plates in elder people. *Surg Radiol Anat* 22:13–19
- Bibby SRS, Jones DA, Lee RB et al (2001) The pathophysiology of the intervertebral disc. *Joint Bone Spine* 68:537–542
- Nachemson A, Lewin T, Maroudas A et al (1970) In vitro diffusion of dye through the end-plates and annulus fibrosus of human lumbar intervertebral discs. *Acta Orthop Scand* 41:589–607
- Roberts S, Urban JPG, Evans H et al (1996) Transport properties of the human cartilage endplate in relation to its composition and calcification. *Spine* 21:415–420
- Accadbled F, Laffosse J-M, Ambard D et al (2008) Influence of location, fluid flow direction, and tissue maturity on the macroscopic permeability of cerebral end plates. *Spine* 33:612–619
- Bernick S, Cailliet R (1982) Vertebral end-plate changes with aging of human vertebrae. *Spine* 7:97–102
- Benneker LM, Heini PF, Alini M et al (2005) Vertebral endplate marrow contact channel occlusions and intervertebral disc degeneration. *Spine* 30:167–173
- Martin MD, Boxell CM (2002) Pathophysiology of lumbar disc degeneration: a review of the literature. *Neurosurg Focus* 13:1–6
- Adams MA, Roughley PJ (2006) What is intervertebral disc degeneration, and what causes it? *Spine* 31:2151–2161
- Ariga K, Miyamoto S, Nakase T et al (2001) The relationship between apoptosis of endplate chondrocytes and aging and degeneration of the intervertebral disc. *Spine* 26:2414–2420
- Lyons G, Einstein SM, Sweet MBE (1981) Biochemical changes in intervertebral disc degeneration. *Biochimica et Biophys Acta* 673:443–453
- Antoniou J, Mwale F, Demers CN et al (2006) Quantitative magnetic resonance imaging of enzymatically induced degeneration of the nucleus pulposus of intervertebral discs. *Spine* 31:1547–1554
- Pfirrmann CWA, Metzdorf A, Elfering A et al (2006) Effect of aging and degeneration on disc volume and shape: a quantitative study in asymptomatic volunteers. *J Ortho Res* 24:1086–1094
- Johannessen W, Auerbach JD, Wheaton AJ et al (2006) Assessment of human disc degeneration and proteoglycan content using T1rho-weighted magnetic resonance imaging. *Spine* 31:1253–1257
- Blumenkrantz G, Zuo J, Li X et al (2010) In vivo 3.0-Tesla magnetic resonance T1rho and T2 relaxation mapping in subjects with intervertebral disc degeneration and clinical symptoms. *Magn Reson Med* 63:1193–1200
- Haase A, Frahm J, Matthaei D et al (1986) FLASH imaging. Rapid NMR imaging using low flip-angle pulses. *JMR* 67(2): 258–266
- Gatehouse PD, He T, Hughes SPF et al (2004) MR imaging of degenerative disc disease in the lumbar spine with ultrashort TE pulse sequences. *MAGMA* 16:160–166
- Dathe H, Helms G (2010) Exact algebraization of the signal equation of spoiled gradient echo MRI. *Phys Med Biol* 55:4231–4245
- Helms G, Dathe H, Dechent P (2008) Quantitative FLASH MRI at 3T using a rational approximation of the Ernst equation. *Magn Reson Med* 59:667–672
- Iatridis JC, Setton LA, Weidenbaum M et al (1997) The viscoelastic behavior of the non-degenerate human lumbar nucleus pulposus in shear. *J Biomech* 30(10):1005–1013
- Rodriguez AG, Slichter CK, Acosta FL et al (2011) Human disc nucleus properties and vertebral endplate permeability. *Spine* 36(7):512–520
- O’Connell GD, Vresilovic EJ, Elliott DM (2011) Human intervertebral disc internal strain in compression: the effect of disc region, loading position, and degeneration. *J Orthop Res* 29(4): 547–555
- Wright AC, Lemdiasov R, Connick TJ et al (2011) Helmholtz-pair transmit coil with integrated receive array for high-resolution

- MRI of trabecular bone in the distal tibia at 7T. *J Magn Reson* 210:113–122
36. Rosset A, Spadola L, Ratib O (2004) OsiriX: an open-source software for navigating in multidimensional DICOM images. *J Digital Imaging* 17:205–216
37. Bae WC, Statum S, Zhang Z et al (2013) Morphology of the cartilaginous endplates in human intervertebral disks with ultra-short echo time MR imaging. *Radiology* 266(2):564–574